Reversible and Selective O$_2$ Chemisorption in a

Porous Metal-Organic Host Material

Journal of the American Chemical Society

Peter D. Southon, David J. Price, Pia K. Nielsen, Christine J. McKenzie and

Cameron J. Kepert

Supporting information

Contents

1. Dioxygen Affinity in Solution

Solution spectrophotometric measurements of [{Co$_2$(O$_2$)(bpbp)}$_2$bdc](ClO$_4$)$_4$ in acetonitrile, acetone, ethanol and methanol were carried out at 40 °C under various O$_2$ partial pressures, P(O$_2$). Argon and dioxygen gas were mixed using two Hastings HFC-202 mass flow controllers and passed into ~0.1 mM solutions (gas flow 30 mL/min) of the complex in a quartz cell (1 cm path length). The gas mixture was bubbled through the solution for 5 min before the measurement to ensure that equilibrium had been reached; longer bubbling times gave identical results. Absorption shoulders, absent in the deoxygenated form, that grow on oxygenation at 380 and 480 nm were monitored. Concentration changes due to solvent loss by evaporation were corrected for by comparing the weight of the cuvette after each measurement to the initial weight. The temperature was controlled using a Shimadzu CPS-240A thermo-electrical temperature controlled cell holder. The equilibrium constant was calculated by the following equation:

$$P(O_2) = C \cdot \frac{P(O_2)}{\Delta A} - K^{-1}$$

where $P(O_2)$ is the partial pressure of O$_2$, ΔA is the difference between the absorbance of the solution at $P(O_2)$ and at $P(O_2)= 0$ atm, while C is a constant.[1,2] A plot of $P(O_2)$ versus $P(O_2)/\Delta A$ gives a straight line from which K^{-1} was determined from the intercept at the y-axis. The binding affinity is given as $P(O_2)_{50\%}= K^{-1}$ and represents the partial pressure of O$_2$ needed to oxygenate 50% of the complex. The strong binding affinity resulted in saturation effects at high $P(O_2)$ and measurements at these partial pressures could not be used in determination of K. Gas mixtures

with $P(O_2)$ lower than ~1.5% could not be obtained without exceeding the calibration range of the flow controllers.

The reversibility of, and affinity for, O_2 binding is similar in acetone, ethanol and methanol, suggesting that these solvents do not compete significantly with O_2 in binding at the Co sites. In contrast, the reversibility of O_2 binding is detrimentally affected if the deoxygenation is carried out in media containing high concentrations of water or in pure water (at low concentration due to insolubility). Water can presumably displace the carboxylate ligand in the Co(II) deoxygenated state, with reoxidation of the resultant aqua complex by O_2 producing the "met" complex $[Co_2(bpbp)(OH)_2(H_2O)_2]^{2+}$, which has been characterized in the solid state as the perchlorate complex and found to be incapable of reversible O_2 binding.[2]

2. Structural refinement details

**Table S1.** Details for the structural solution of **1**·2O$_2$

formula	C$_{80}$H$_{84}$Co$_4$F$_{24}$N$_{12}$O$_{10}$P$_4$
FW	2187.18 g mol^{-1}
T	100(2) K
crystal system	Monoclinic
space group	$P2_1/n$
a	10.225(2) Å
b	12.729(3) Å
c	36.869(7) Å
β	93.70(3)°
V	4788.7(16) Å^3
ρ_{calc}	1.517 Mg m^{-3}
Z	2
μ	0.854 mm^{-1}
data / restraints / parameters	7571 / 0 / 613
$R_1(F^2)$ [$I>2\sigma(I)$, all]	0.0904, 0.0968
$wR_2(F^2)$ [$I>2\sigma(I)$, all]	0.2587, 0.2658
GoF	1.025
Solvent-accessible void volume	646.8 Å^3

Analysis of the diffuse difference electron density in the void regions of the structure using PLATON/SQUEEZE gave a value of 62 electrons per unit cell. We attribute this non-zero value principally to systematic errors in the low angle diffraction data, as reflected in the relatively high refinement indices, rather than to any appreciable retention of water in the crystal. This conclusion is supported by the excellent agreement between the unit cell parameters for this structure and those determined by indexing the synchrotron-PXRD pattern for **1**·$2O_2$, and disagreement with those for **1**·$2O_2$·$3H_2O$.

3. Thermogravimetric measurements
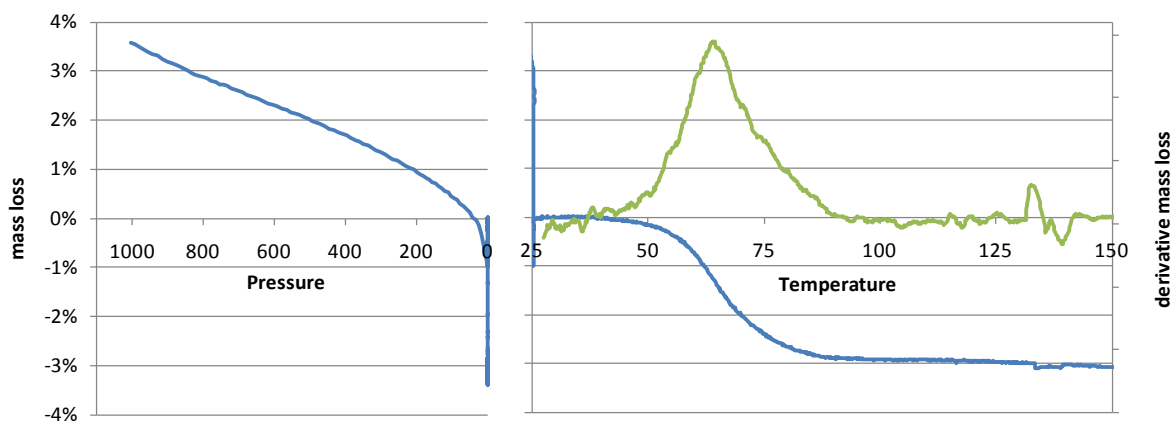
Figure S1. Vacuum thermogravimetry for $1 \cdot 2O_2 \cdot 3H_2O$. Mass loss was normalized to the mass after complete evacuation, assumed to be the desolvated state. The green line is the differential of mass change, with respect to temperature.
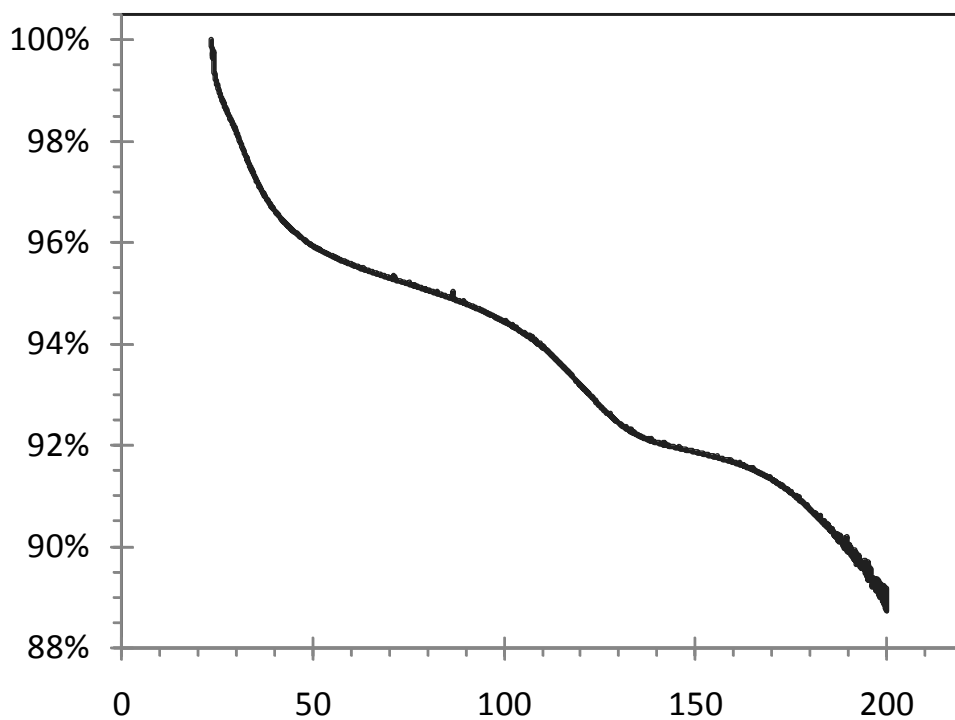
Figure S2. Thermogravimetric analysis of $1 \cdot 2O_2 \cdot 3H_2O$ under flowing N_2.

4. Adsorption isotherms at 25°C

Kinetics

Gravimetric measurement of isotherms allows adsorption and reaction kinetics to be measured. At each point of the isotherm the mass is monitored for a minimum time period, which may be extended if absorption is not complete. The change in mass as a function of time can be fitted with a model to determine a time constant and a projected asymptote.

In this case the linear driving force model[3] was used, expressed in the form

$$m(t) = m_0 + \Delta m \left(1 - e^{-\left[\frac{(t - t_0)}{k} \right]} \right)$$

where $m(t)$ is the sample mass as a function of time, t, m_0 is the mass at the arbitrary time origin t_0, k is the time constant, and Δm is the change in uptake. The asymptotic mass is then equal to $m_0 + \Delta m$.

It was observed that when dosing **1** with O_2 from vacuum to a pressure above the saturation point (approx. 5 mbar), uptake is very rapid; modeling to the linear driving force model gives a typical time constant of 5.5 minutes. However, when dosing at pressures below 5 mbar the kinetics are much slower, with time constants well over 5 hours.
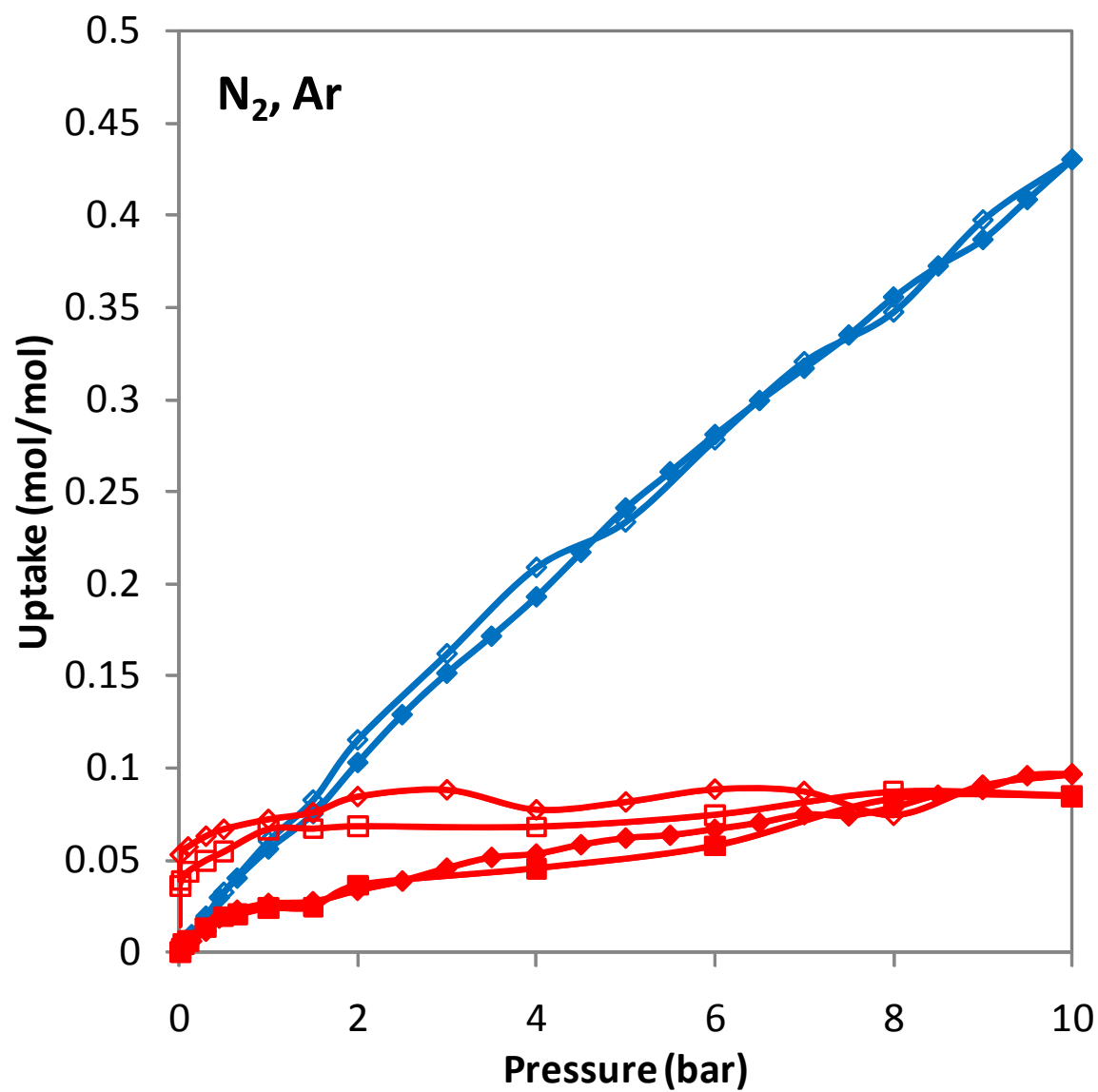
Isotherms
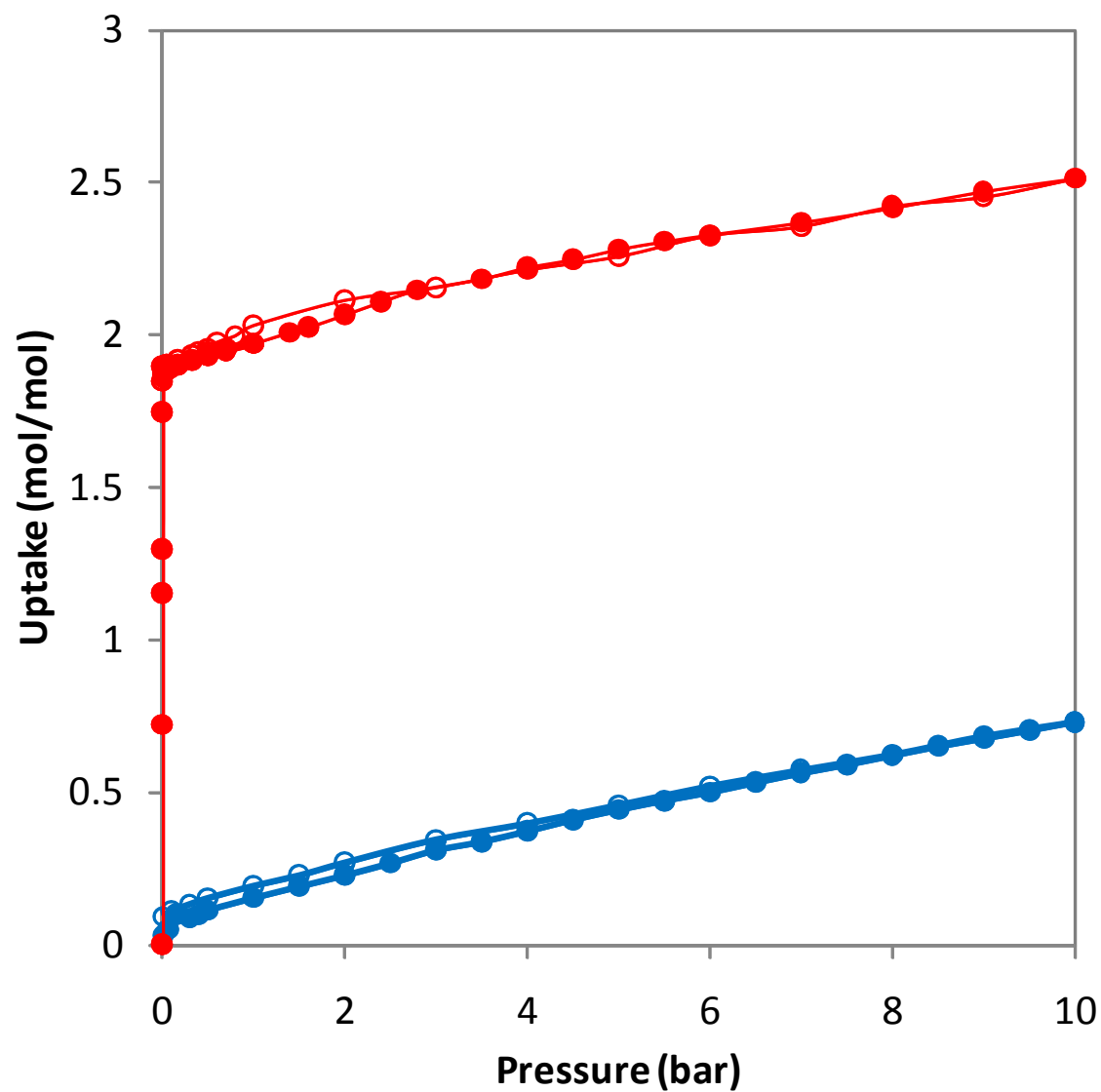
Figure S3. Adsorption isotherms of O_2 on **1** (red) and **1**·$2O_2$ (blue) at 25 °C to 10 bar. Data points measured on desorption are indicated by unfilled symbols.
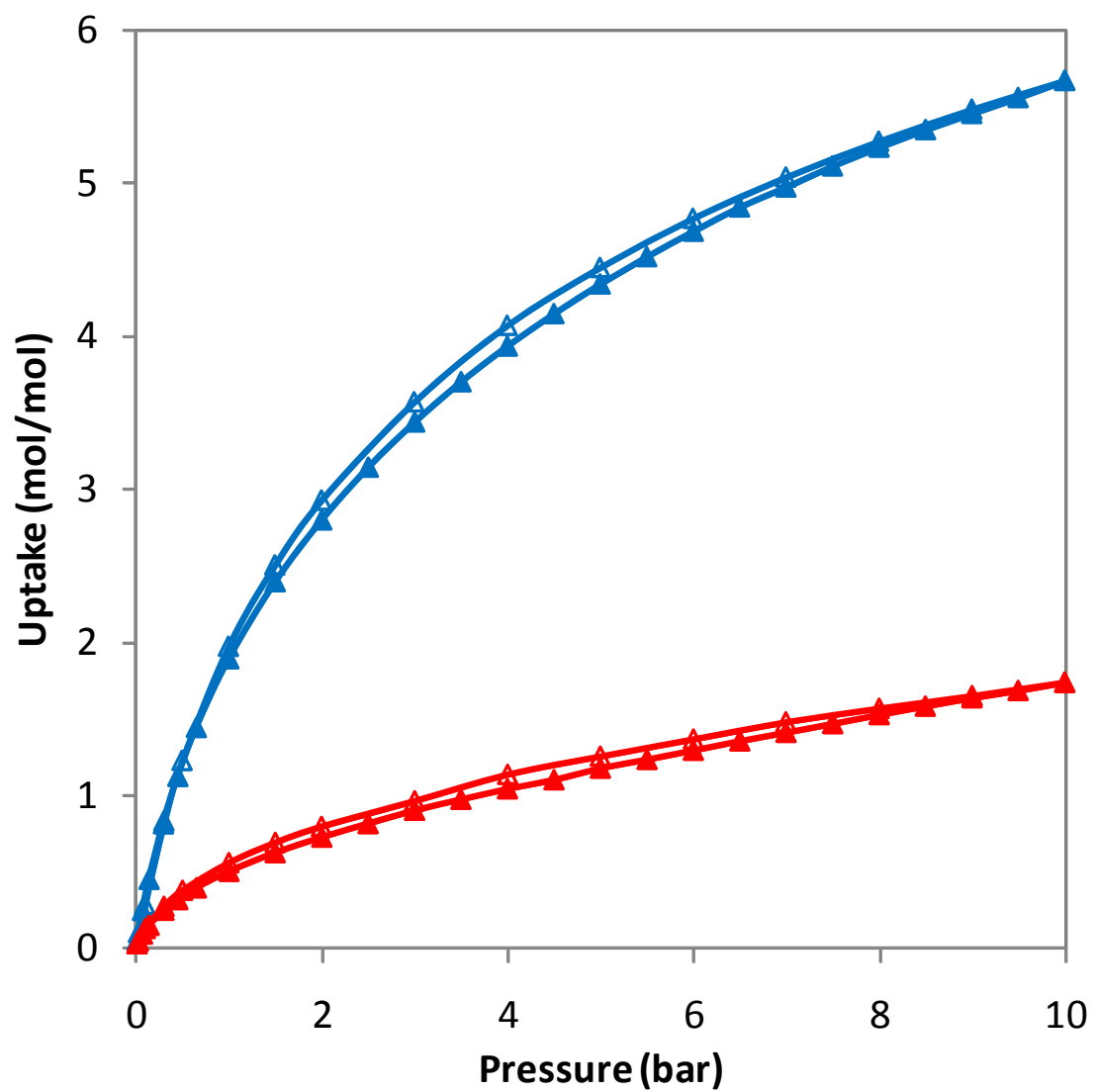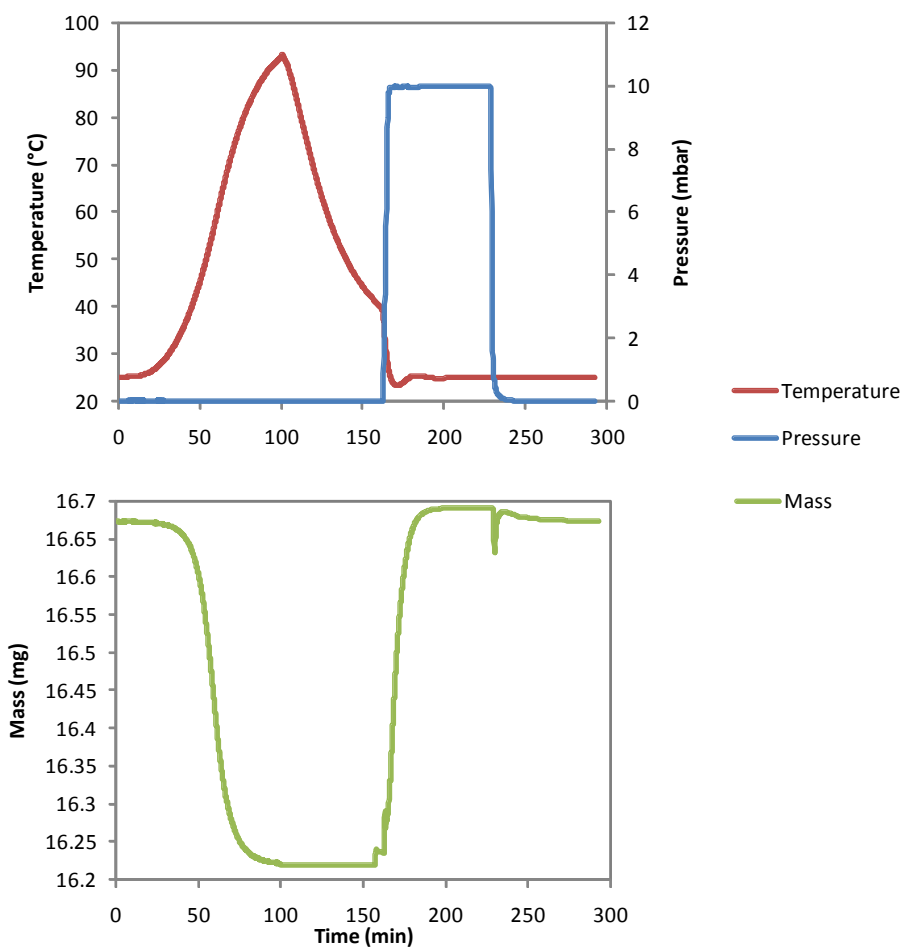
Figure S4. Adsorption isotherms of CO_2 on **1** (red) and **1**·$2O_2$ (blue) at 25 °C to 10 bar. Data points measured on desorption are indicated by unfilled symbols.
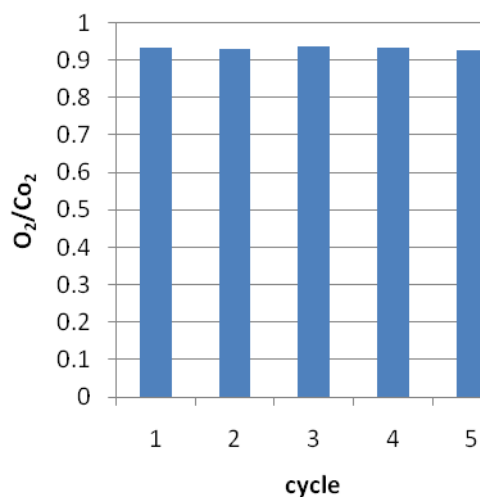
Figure S5. Adsorption isotherms of N_2 (♦) and Ar (■) on **1** (red) and **1**·$2O_2$ (blue) at 25 °C to 10 bar. Data points measured on desorption are indicated by unfilled symbols.

5. Dioxygen sorption/desorption cycles


Figure S6. Typical desorption/sorption cycle.

Figure S7. O$_2$ uptake at 10 mbar and 25 °C over 5 desorption/sorption cycles.

6. Low temperature isotherms

Experimental details. Dinitrogen (at 77 K) and argon (at 77 and 87 K) adsorption isotherms were measured on both oxygenated and deoxygenated forms. The first N_2 isotherm was measured on $\mathbf{1} \cdot 2O_2$ after evacuation at 40°C to remove solvent, then after heating at 85°C to remove O_2 isotherms for both N_2 and Ar were measured at 77 K. For the Ar measurements at 87 K, the sample was heated under vacuum to remove both solvent and O_2 before the first isotherm was measured, then exposed to 100 mbar of O_2 and a second isotherm measured.
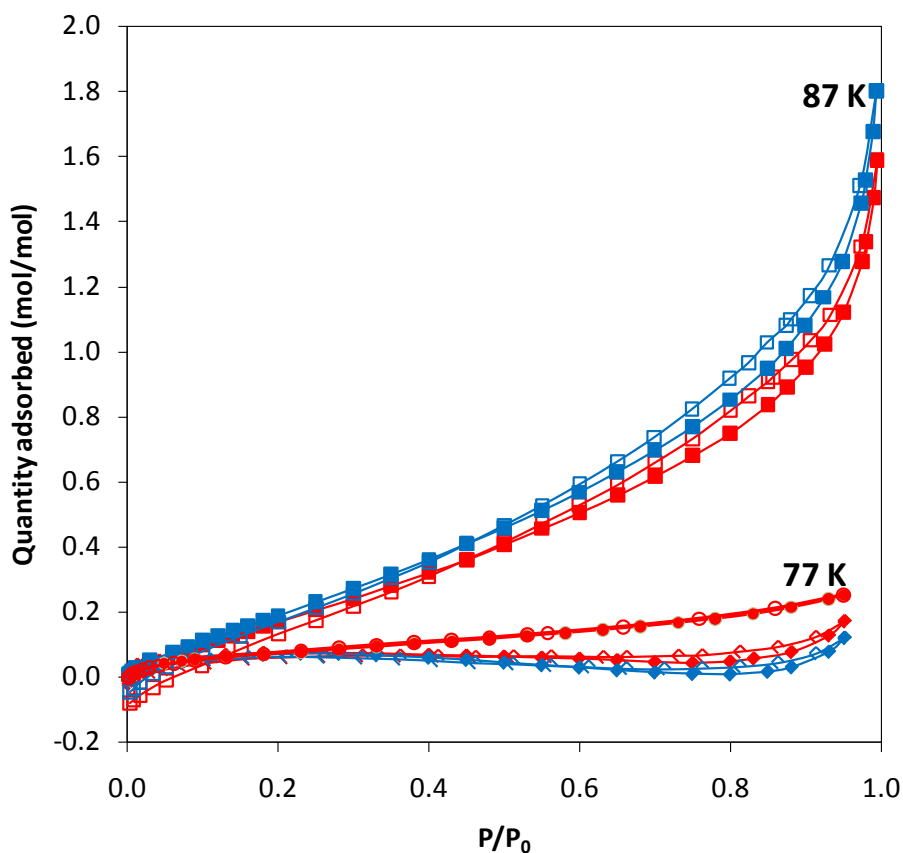
**Figure S8.** Adsorption isotherms of N_2 (measured at 77 K, ♦) and Ar (measured at 77 (●) and 87 K (■)) on **1** (red) and $\mathbf{1} \cdot 2O_2$ (blue), expressed as molar ratio. Data points measured on desorption are indicated by unfilled symbols.
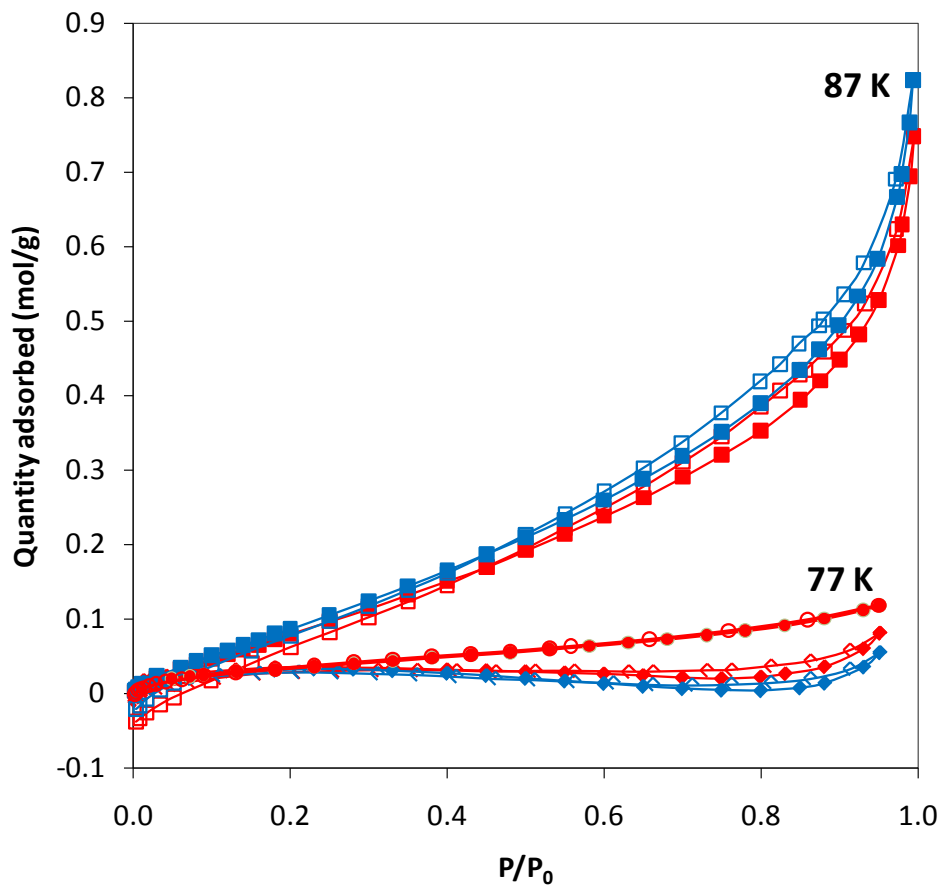
Figure S9. Adsorption isotherms of N_2 (measured at 77 K, ♦) and Ar (measured at 77 (●) and 87 K (■)) on **1** (red) and **1**·$2O_2$ (blue), expressed as moles adsorbed per gram adsorbent. Data points measured on desorption are indicated by unfilled symbols.

7. High temperature isotherms
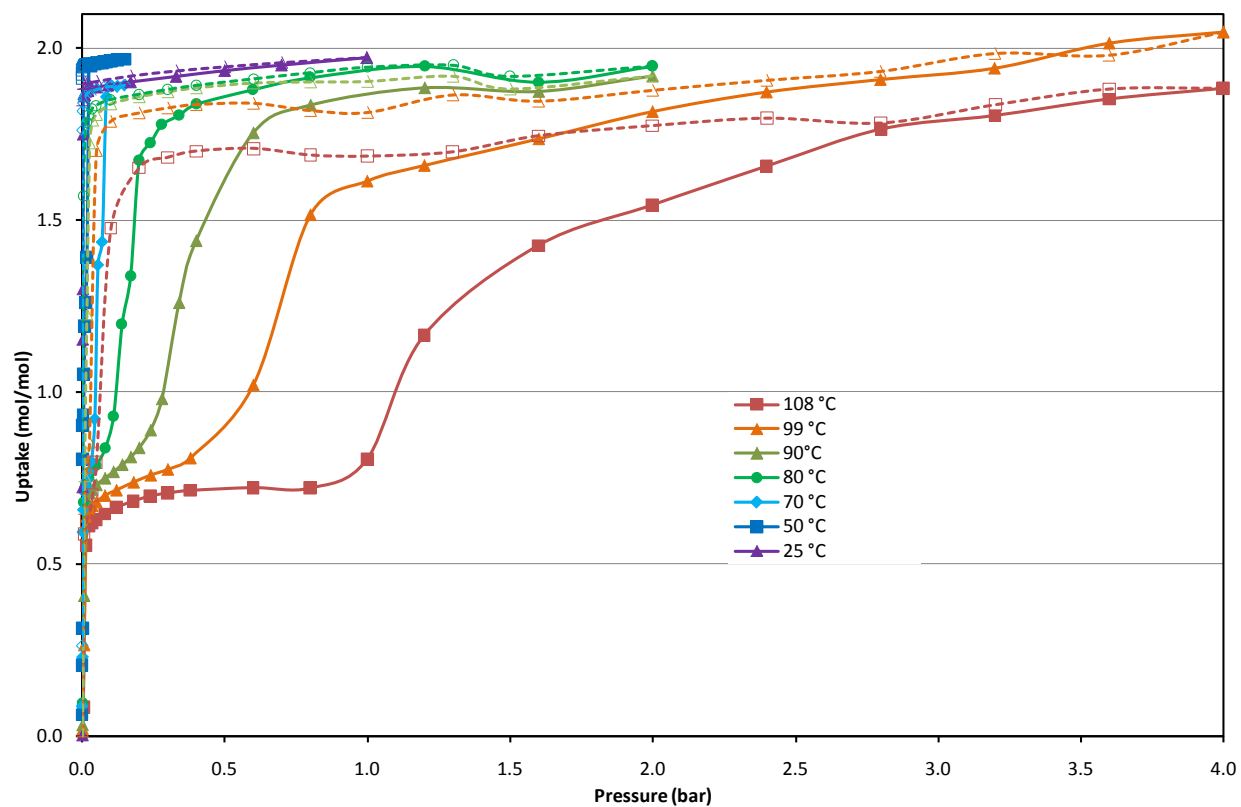
Figure S10. Full isotherms for O_2 on **1** at 25, 50, 70, 80, 90, 99 and 108 °C. Unfilled data points were measured during desorption. The 50 °C isotherm was measured on a different samples, which gave a marginally higher saturation uptake compared to the other isotherms.
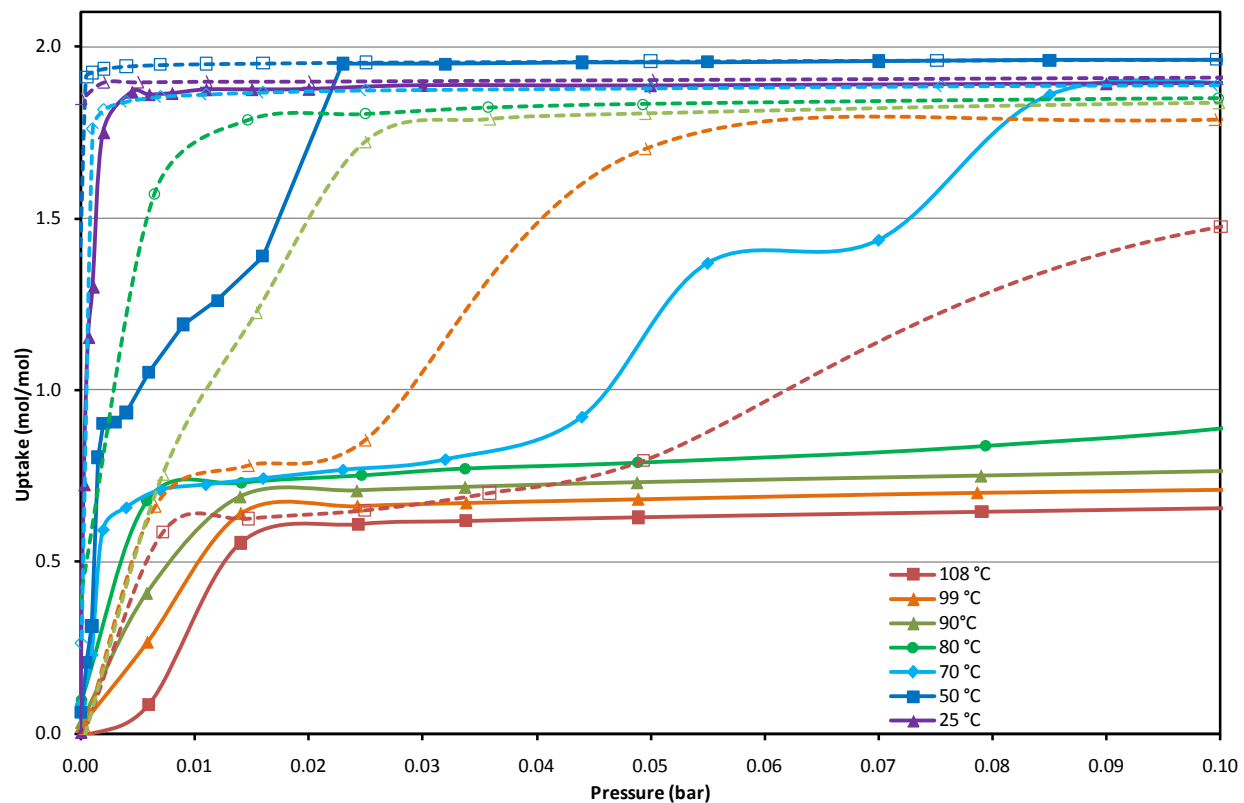
Figure S11. Low pressure detail of the isotherms for O_2 on **1** at 25, 50, 70, 80, 90, 99 and 108 °C. Unfilled data points were measured during desorption.

8. Calculation of enthalpies from high temperature isotherms

Dioxygen isotherms were measured in the temperature range 50-108 °C. Calculations of the enthalpy of binding (ΔH) used the Clausius-Clapeyron relation, which defines ΔH in terms of pressure (P) and temperature (T) at a given surface coverage (θ)

$$\Delta H = -R \left(\frac{\delta \ln P}{\delta T^{-1}} \right)_\theta$$

Where sorption isotherms are measured at two or more temperatures, plotting $\ln P$ vs $1/T$ at a given uptake (n) (which is assumed to be equivalent to θ) will give ΔH according to the equation

$$\ln P = -R\Delta H(T^{-1}).$$

These plots, referred to as adsorption isosteres, are shown in Figure S12. This method is essentially equivalent to a van't Hoff plot.

Loadings part-way though each stage of uptake were chosen: 0.3 mol/mol for the first stage, and 0.95, 1.2 and 1.6 mol/mol for the second stage. The corresponding pressure at each loading was interpolated from the isotherm data. Pressures less than ca. 2 mbar were omitted from the Clausius-Clapeyron analysis, due to significant uncertainty in their value, but are plotted in Figure S12 for completeness. As the main source of uncertainty is in the interpolation of pressure values from the data, which is difficult to estimate, errors are not shown on the plot. Calculated values for the enthalpy of adsorption are given in Table S2.

The data set for 0.95 mol/mol was used to extrapolated the value of $P(O_2)_{50\%}$ in the solid state at 40 °C (plotted as a purple triangle in Figure S12), for comparison with the $P(O_2)_{50\%}$ value measured in solutions (orange triangle).
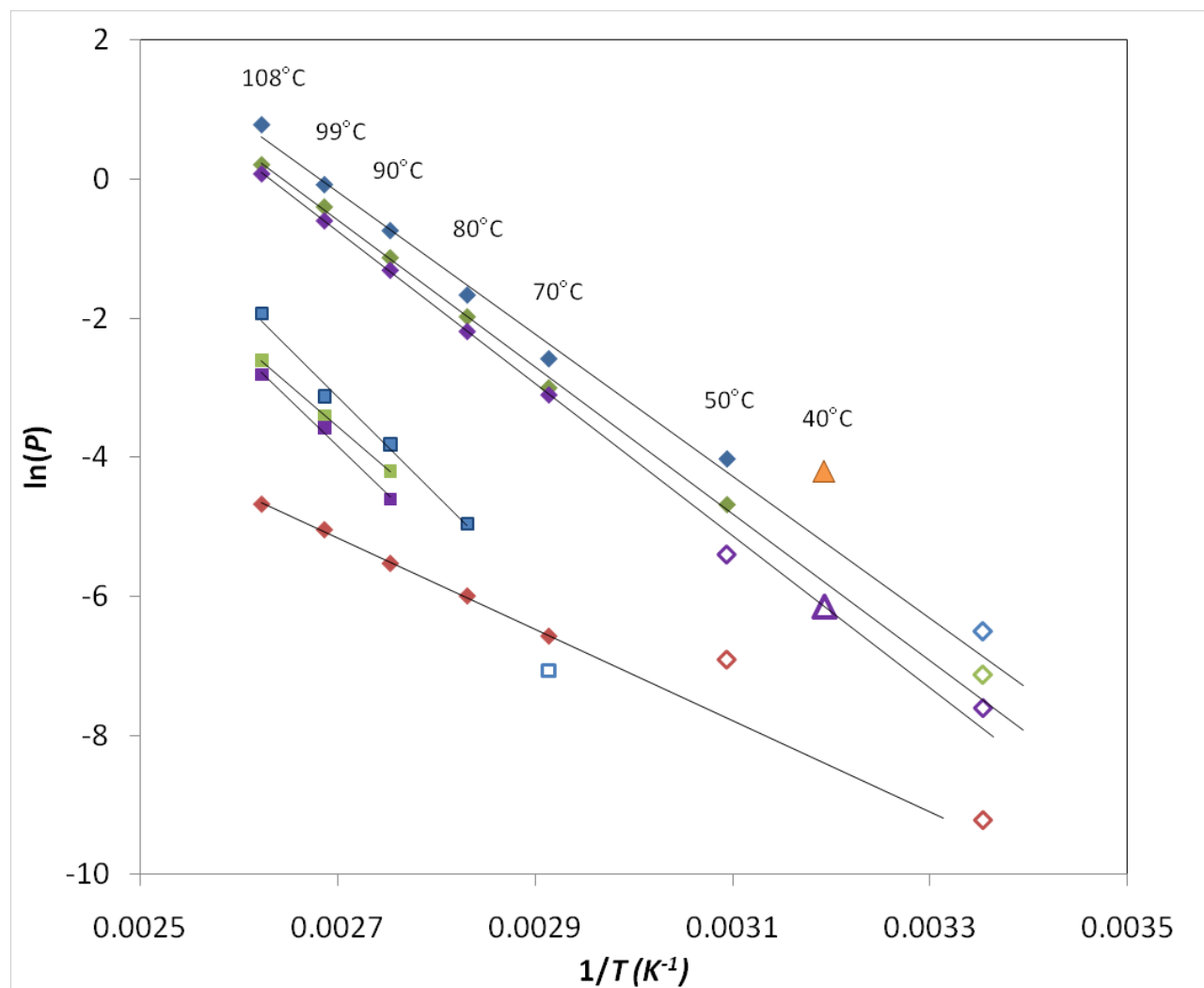
Figure S12. Clausius-Clapeyron plot for loadings of 0.3 mol/mol (red), 0.95 mol/mol (purple), 1.2 mol/mol (green), and 1.6 mol/mol (blue). Data points from sorption curves are diamonds, and points from desorption curves are squares. Unfilled data markers were not used to calculate enthalpy values, due to high estimated uncertainty in the low pressure values, but are shown for completeness. The orange triangle indicates the measurement of $P(O_2)_{50\%}$ in acetonitrile solution at 40 °C. The purple triangle indicates the value of $P(O_2)_{50\%}$ in the solid state at 40 °C, extrapolated from the 0.95 mol/mol data set.

Table S2. Calculated values for the enthalpy of binding.

| Stage	Loading (mol·mol^{-1})	Enthalpy of binding (kJ·mol^{-1})	
1st stage, sorption	0.3	-55	◆
2nd stage, sorption	0.95	-91	◆
	1.2	-88	◆
	1.6	-85	◆
average		-88	
2nd stage, desorption	0.95	-115	■
	1.2	-102	■
	1.6	-118	■
average		-112	

9. Colour change with doxygenation

Figure S13. Photo of the oxygen-binding complex on a temperature-gradient hot plate.

10. Visible-NIR spectra

The diffuse-reflectance visible-NIR spectrum of $1 \cdot 2O_2 \cdot 3H_2O$, shown in Figure S14, was measured with a Cary 5 UV-vis spectrometer, with a Harrick Omni-Diff probe. The powder was smeared onto high density filter paper onto which the Omni Diff Probe was placed.
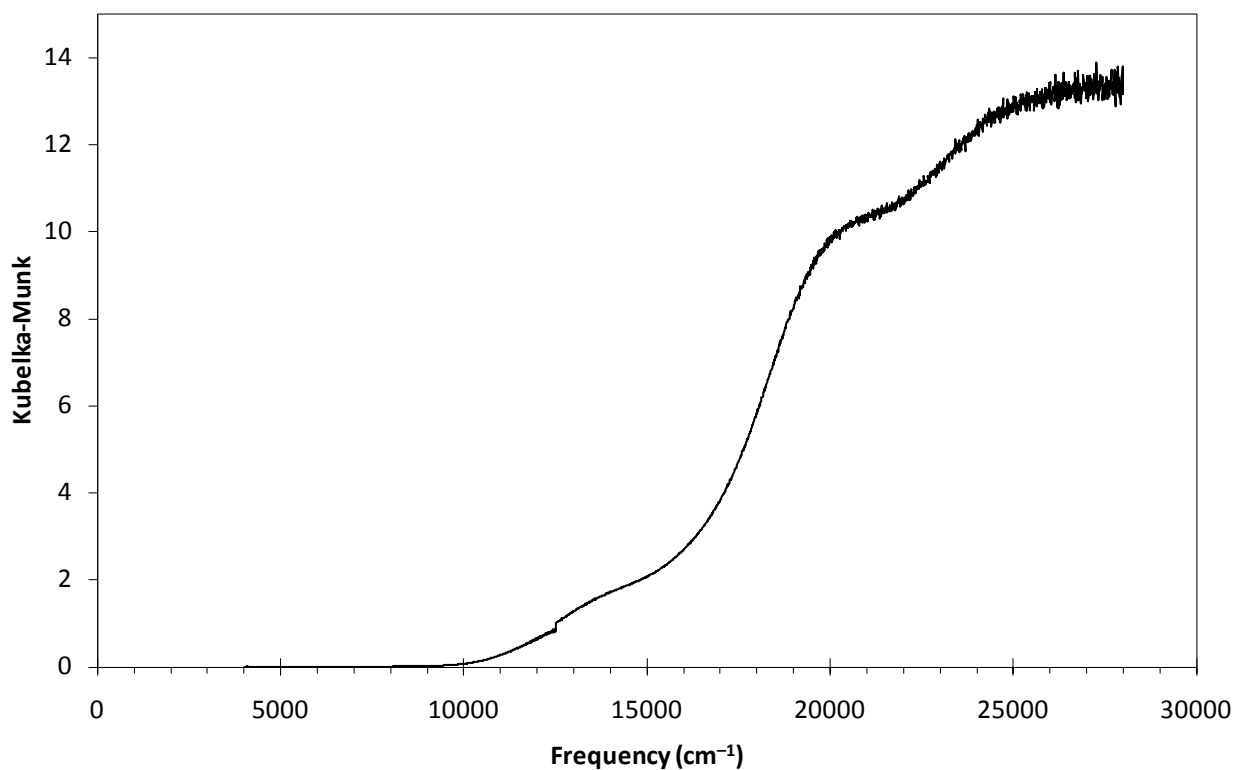

Figure S14. The visible-NIR spectrum of $1 \cdot 2O_2 \cdot 3H_2O$.

11.   Raman spectroscopy

Samples of $1 \cdot 2O_2 \cdot 3H_2O$, $1 \cdot O_2$, and 1 were prepared in sealed glass capillaries, as described for Synchrotron Powder X-ray Diffraction. Raman spectra, using an excitation frequency of 488 nm, were measured with a Renishaw Raman System 2000. The collection optics were based on a Leica DMLM microscope with a ×50 objective, allowing Raman spectra to be collected from small spots on the surface of crystals. To minimize heating of the sample, risking desolvation or deoxygenation, the laser power was reduced and the sample spot was shifted with each exposure; however, the existence of such effects cannot be entirely discounted. The Raman spectra presented are summed from spectra measured at different spots on several crystals.

Summed spectra of $1 \cdot 2O_2 \cdot 3H_2O$, $1 \cdot O_2$, and 1 are given in Figure S15. Only minor differences were observed between them, and at this point we are not able to assign any of these changes with confidence.
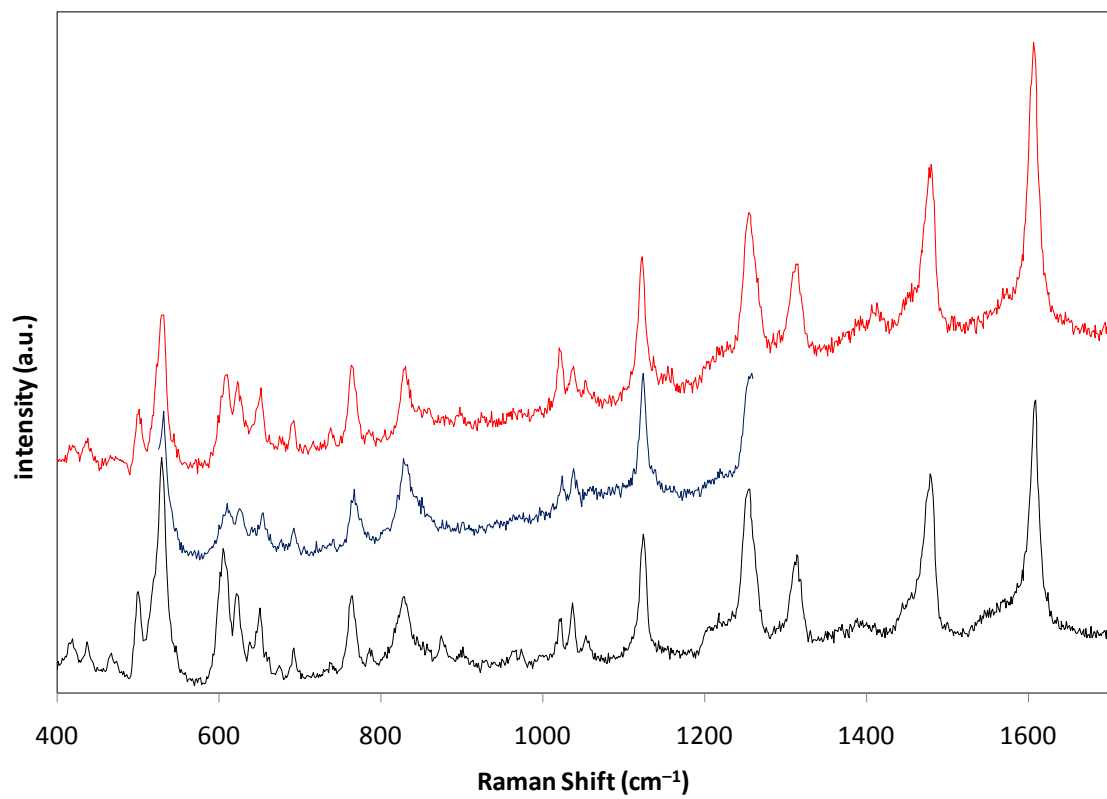
Figure S15. Raman spectra of $\mathbf{1}\cdot 2O_2\cdot 3H_2O$ (black), $\mathbf{1}\cdot O_2$ (blue), and $\mathbf{1}$ (red).

12. References

(1) Rose, N. J.; Drago, R. S. *J. Am. Chem. Soc.* **1959**, *81*, 6138.

(2) Collman, J. P.; Brauman, J. I.; Doxsee, K. M.; Halbert, T. R.; Hayes, S. E.; Suslick, K. S. *J. Am. Chem. Soc.* **1978**, *100*, 2761.

(3) Sircar, S.; Hufton, J. R. *Adsorpt.-J. Int. Adsorpt. Soc.* **2000**, *6*, 137.